

Article

Deformation of Sandy Ground Induced by Tunneling of Super-Large-Diameter Shield—Influence of Buried Depth of Tunnel and Relative Density of Sand

Jiquan Li ¹, Xiaolu Li ², Yuqin Wen ^{3,4} and Dong Su ^{3,*} ¹ Foshan Jianying Development Co., Ltd., Foshan 528313, China² Guangdong Provincial Transport Planning and Research Center, Guangzhou 510101, China³ College of Civil and Transportation Engineering, Shenzhen University, Shenzhen 518060, China⁴ Shenzhen Longhua Construction Development Co., Ltd., Shenzhen 518110, China

* Correspondence: sudong@szu.edu.cn; Tel.: +86-0755-2653-5204

Abstract: The mechanical properties of sandy soil depend on both the confining pressure and the state of compactness. Therefore, both the buried depth of the tunnel and the relative density of the sand are key factors that affect the ground deformation induced by the tunneling of a super-large-diameter shield. In this study, the parameters of the SANISAND constitutive model are first calibrated based on triaxial test data for Foshan silty fine sand. Then, based on the actual project, a two-dimensional finite-element analysis model is established to investigate the ground deformation induced by the tunneling of a super-large-diameter shield. The width and maximum value of the settlement trough, the volume loss ratio, and the deformation characteristics of the soil are summarized and analyzed for 13 cases. The results show that as the ratio of the buried depth to the diameter and the relative density of sand increases, the anti-disturbance ability of the sand layer to the tunnel construction increases and the volume loss ratio of the stratum reduces correspondingly. The denser the sand and the smaller the confining pressure of the soil around the tunnel, the more significant the shear-induced expansion of the sand at the tunnel haunch; this expansion partially makes up the volume loss caused by the tunnel excavation and reduces the loss ratio of the stratum at the arch crown.



Citation: Li, J.; Li, X.; Wen, Y.; Su, D. Deformation of Sandy Ground Induced by Tunneling of Super-Large-Diameter Shield—Influence of Buried Depth of Tunnel and Relative Density of Sand. *Symmetry* **2023**, *15*, 71. <https://doi.org/10.3390/sym15010071>

Academic Editor: Rafal Grzejda

Received: 27 November 2022

Revised: 20 December 2022

Accepted: 23 December 2022

Published: 27 December 2022



Copyright: © 2022 by the authors. Licensee MDPI, Basel, Switzerland. This article is an open access article distributed under the terms and conditions of the Creative Commons Attribution (CC BY) license (<https://creativecommons.org/licenses/by/4.0/>).

Keywords: sand; super-large-diameter tunnel; volume loss ratio; relative density; buried depth

1. Introduction

With the development of urbanization and rapid increases in the population densities of cities, the traffic demand has increased, and the construction of roads and bridges can no longer meet requirements due to limited ground space. The construction of tunnels, which make use of the underground space of urban cities, has become a promising way to solve this problem and promote the sustainable development of cities. For the construction of tunnels, shield tunneling has been widely adopted for its versatility in complex geological conditions and good performance in controlling the ground surface deformation and safety of the surrounding environment during excavation [1]. However, in the case of super-large-diameter shield tunnels, it is more difficult to control the soil deformation on the ground and at the tunnel face, as the ratio of the shield's buried depth to its diameter is relatively small generally.

In the past, many scholars studied shield tunneling in ground consisting of various soils and investigated the ground deformation due to tunnel excavation. Using field measurements, Peck [2] found that the transverse settlement trough of the ground caused by tunnel excavation can generally be described by a Gaussian distribution curve. With the continuous development and progress of tunnel engineering, in order to better apply the Peck formula to predict ground deformation caused by tunneling, scholars have modified the Peck formula according to soil layer properties, construction parameters, and

deformation requirements. Fattah et al. [3] adopted analytical, empirical, and numerical solutions to investigate the shape of the settlement trough induced by tunneling in cohesive ground. Generally, the Peck formula was unsuitable for a shallow-buried tunnel, so Song et al. [4] proposed a simple and accurate prediction approach for surface settlement, which involved improving the Peck method based on the basic idea of stochastic medium theory. Zhou et al. [5] built up a database consisting of 16 tunnel excavation projects in clayey soils. Based on the database, a serviceability performance function was proposed based on the Peck formula, and the influence of the ground loss ratio and fitting parameters on the failure probability was evaluated. As seepage is ubiquitous during tunneling in grounds with high groundwater tables, Wei et al. [6] established a groundwater seepage and drainage model of a tunnel. The influence of seepage on the effective stress of the soil layer around the tunnel was analyzed, and a calculation formula for the ground settlement considering seepage flow was derived based on the Peck formula. Tang et al. [7] proposed a modified Peck formula considering geological conditions to improve the accuracy of the surface settlement prediction of twin tunnels. In practice, due to the different excavation sequences, an asymmetric disturbance is generated by the construction of twin parallel tunnels. A modified Peck formula suitable for considering the influence of the preceding tunnel on the subsequent tunnel was proposed by Li et al. [8].

In addition to empirical formulas, the finite element method has been adopted by many scholars to establish numerical models by which to simulate tunnel excavation, and the results are generally compared with predictions using empirical formulas [9–12]. Zhang et al. [13] described the performance of the Peck formula in predicting the transverse surface settlement trough in a sandy cobble layer, and the influence of shield tunneling on the transverse and longitudinal ground deformation was estimated using numerical simulation and analytical analyses. Zhang et al. [14] established a three-dimensional numerical model of tunneling to analyze the ground settlement and used Peck's formula to determine the width coefficient of the settlement trough and the loss rate of the sand-mixed stratum.

Physical model testing has been adopted by many scholars to simulate the tunnel excavation process in various soil layers. Fang et al. [1] carried out model testing and observed that two major factors influence the longitudinal settlement of the ground surface, i.e., the buried depth of the tunnel and the loss of surface soil. The results of the scaled-model testing by Hu et al. [15] showed that the water content of sand has a significant influence on the settlement of the surface and deep soil layer. Moussaei et al. [16] carried out model tests to simulate the excavation process for a single circular tunnel and explored the surface deformation caused by shield tunneling in sandy soils with three cover/diameter ratios of the tunnel and four different densities. Based on digital image correlation (DIC) technology, transparent sand was adopted by Sun et al. [17] to investigate the shape of the settlement trough under different buried depths of the tunnel. The results show that the width of the settlement trough decreases with the increase in buried depth, and the disturbance zone of the soil layer changes from "trapezoid + rectangle" to "trapezoid + bell". Lu et al. [18] studied three-dimensional surface settlement caused by tunnel excavation under different cover/diameter ratios using centrifuge testing and found that the influence range of surface settlement along the tunneling direction is within 1.25 times the diameter from the tunnel excavation face.

Most of the above studies focused on medium-diameter to large-diameter shield tunnels, but few studies have investigated the ground deformation of the sand soil layer caused by the excavation of super-large-diameter tunnels. In addition, the constitutive models used in previous numerical studies seldom consider the differences in mechanical properties of sand under different confining pressures and relative densities. Therefore, the advanced soil constitutive models were adopted necessarily to systematically study the ground deformation induced by the construction of super-large-diameter shield tunnels.

In this study, the characteristics of ground deformation induced by the construction of a super-large-diameter tunnel are investigated, based on the Jihuaxi Road tunnel project in

Foshan of Guangdong province, China. The tunnel is mainly buried in ground consisting of silty sand, with a buried depth ranging from 0.8 to 3 times the tunnel diameter. The research presented in this manuscript can be divided into three stages. Firstly, the parameters of the SANISAND constitutive model are first calibrated based on the triaxial test data for Foshan silty fine sand. Then, based on two-dimensional numerical analyses, the influence of the ratio of the buried depth of the tunnel to the diameter and the relative density of the sand on ground deformation as induced by shield tunneling are studied. Finally, the impact of the ratio of the buried depth to the diameter and the relative density of the sand on the parameters of Peck's formula is analyzed, and a formula for estimating the main parameters of the settlement curve is obtained.

2. Calibration of SANISAND Constitutive Model by Triaxial Test

SANISAND is an elastoplastic model of sand controlled by stress ratio and considering critical state and shear dilatancy. By changing several values of a set of constitutive model parameters, the behavior of sand under different compactness and stress conditions can be achieved. The stress-strain relationship of the constitutive model can be described as follows [19]:

$$d\varepsilon_q^e = \frac{dq}{3G}; d\varepsilon_v^e = \frac{dp}{K} \quad (1)$$

$$d\varepsilon_q^p = \frac{d\eta}{H}; d\varepsilon_v^p = d \left| d\varepsilon_q^p \right| \quad (2)$$

G and K are elastic shear and bulk incremental moduli, respectively. H is the plastic hardening modulus associated with the increment in stress ratio $d\eta$. Whereas p is the mean normal stress, q is the deviatoric stress; ε_q and ε_v are the deviatoric and volumetric strain, respectively. In addition, the superscripts e and p represent the elastic and plastic parts of the strain, respectively.

Since deviatoric plasticity occurs only when $d\eta = 0$, Equation (2), a stress-ratio-defined yield surface should be proposed as follows:

$$f = |\eta - \alpha| - m = 0 \quad (3)$$

Equation (3) represents geometrically a “wedge” in p - q space, shown by the shaded area in Figure 1, whose bisecting line has a slope α , and the wedge opening a value of $2mp$. The α and m are stress ratio quantities. When η satisfies Equation (4) and $d\eta$ points “outward” from the wedge, i.e., $d\eta > 0$ at the upper and $d\eta < 0$ at the lower wedge lines, plasticity occurs according to Equation (2).

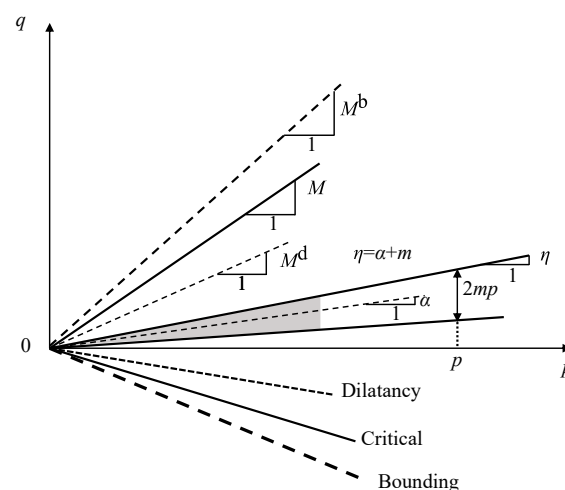


Figure 1. Schematic of the yield, critical, dilatancy, and bounding lines in q - p space.

In this study, the constitutive model, SANISAND, is adopted. Due to the high permeability coefficient of sand, the in situ sand layer has been consolidated under gravity. As the loading rate induced by shield tunneling is relatively low which allows the complete dissipation of excess pore water pressure, consolidated drained (CD) tests are adopted to calibrate the model parameters. The samples are prepared by compaction of sand layer by layer in the laboratory so that its void ratio is close to that of in situ soil. The physical characteristics of silty fine sand are shown in Table 1.

Table 1. Physical characteristics of silty fine sand.

Soil	State	e_{\min}	e_{\max}	G_s	C_u	C_c	ν	E_0
Silty fine sand	Loose	0.686	1.107	2.62	5.33	3.52	0.32	4.5

The main parameters for the SANISAND model include the elastic parameters and the critical state parameters.

(1) Elastic parameters

Among the parameters of the SANISAND constitutive model, the elastic parameters include the shear modulus constant G_0 and Poisson's ratio ν . Poisson's ratio can be taken as $\nu = 0.2$ for silty sand and the shear modulus constant G_0 is determined by the following equation:

$$G_0 = \frac{(1+e)}{3\sqrt{p'P_{at}}(2.97-e)^2} \frac{Dq}{D\varepsilon_q^e} \quad (4)$$

where e is the void ratio, p' is the effective mean normal stress, P_{at} is the atmospheric pressure, and ε_q^e is the elastic component of the deviator strain.

According to Taiebat and Dafalias [20], the calibration of G_0 should be based on the measured relationship between the deviatoric stress q and the deviatoric strain ε_q when ε_q is less than 0.1%. Figure 2 presents the results obtained from the triaxial drain test with a confining pressure of 100 kPa. Compared with the relevant research [19–21], the value of G_0 can be taken as 120.

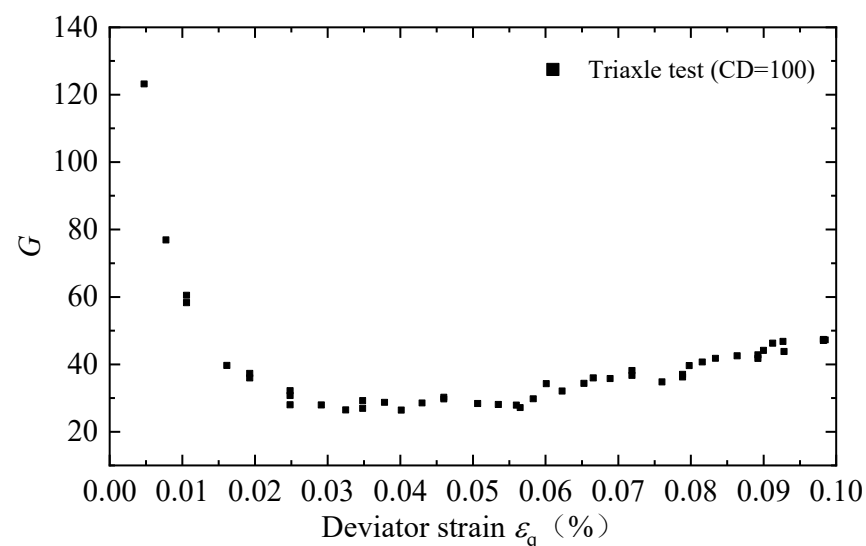


Figure 2. Calibration of shear modulus constant G_0 .

(2) Critical state parameters

In the SANISAND model, the critical state parameters include the critical state stress ratio and the critical state line. The critical state stress ratio is M_c under triaxial compression.

To determine the critical state stress ratio M_c , triaxial consolidation drain tests were conducted under different confining pressures and the results are presented in Figure 3. It can be seen from the figure that when the soil reaches the critical state, its stress ratios are 1.39, 1.32, and 1.30 for confining pressures of 100, 200, and 400 kPa, respectively. The average value, i.e., 1.33, is adopted for the parameter M_c in the numerical analyses.

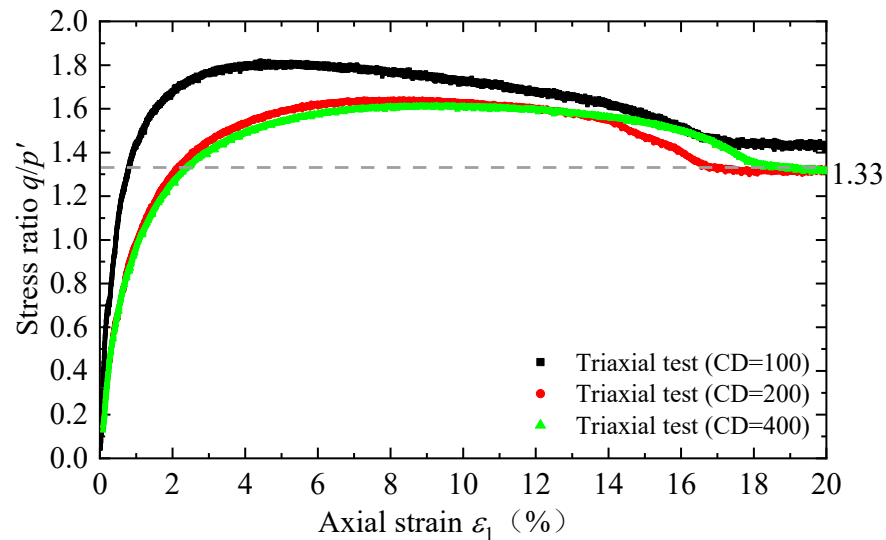


Figure 3. Calibration of the critical state stress ratio M_c .

As shown in Equation (5), the critical state line of soil in the $e-p'$ plane is determined by the parameters e_0 , λ , c , and ζ .

$$e_c = e_0 - \lambda_c \left(\frac{p_c}{P_{at}} \right)^\zeta \tag{5}$$

According to Dafalias and Manzari [19] and, Taiebat and Dafalias [20], it can be assumed that $\zeta = 0.7$. Then, based on the relationship between the void ratio and the effective stress when the soil reaches the critical state during the triaxial tests, the critical state line CSL1 can be determined, as shown in Figure 4. The calibrated values are $e_0 = 1.014$ and $\lambda_c = 0.036$.

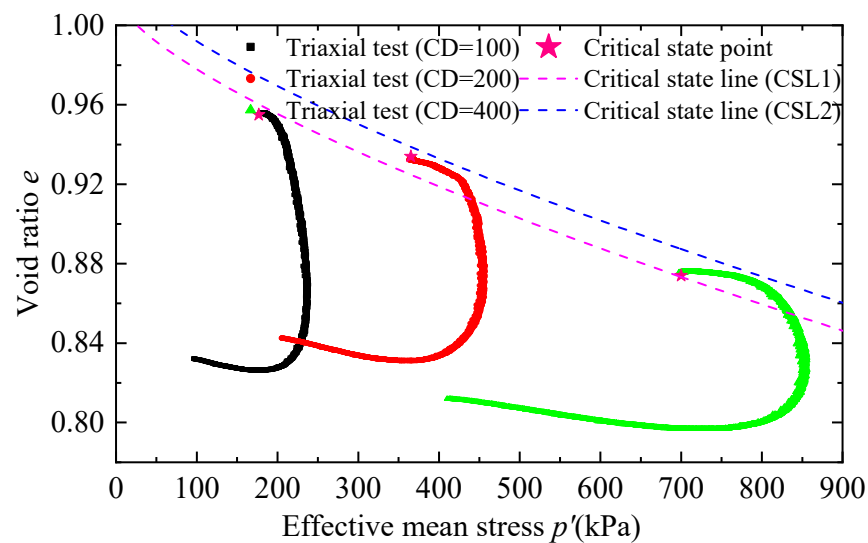


Figure 4. Calibration of critical state line (CSL).

However, a shear band was formed in the specimen during some tests, which led to a certain error in the measured void ratio in the critical state. For this reason, the parameter e_0 was slightly adjusted until the overall responses of sand during the triaxial tests were successfully reproduced. It was found that the calculated and measured results match well when $e_0 = 1.024$, as shown in Figure 5; therefore, the adopted critical state parameters are $\zeta = 0.7$, $e_0 = 1.024$, and $\lambda_c = 0.036$.

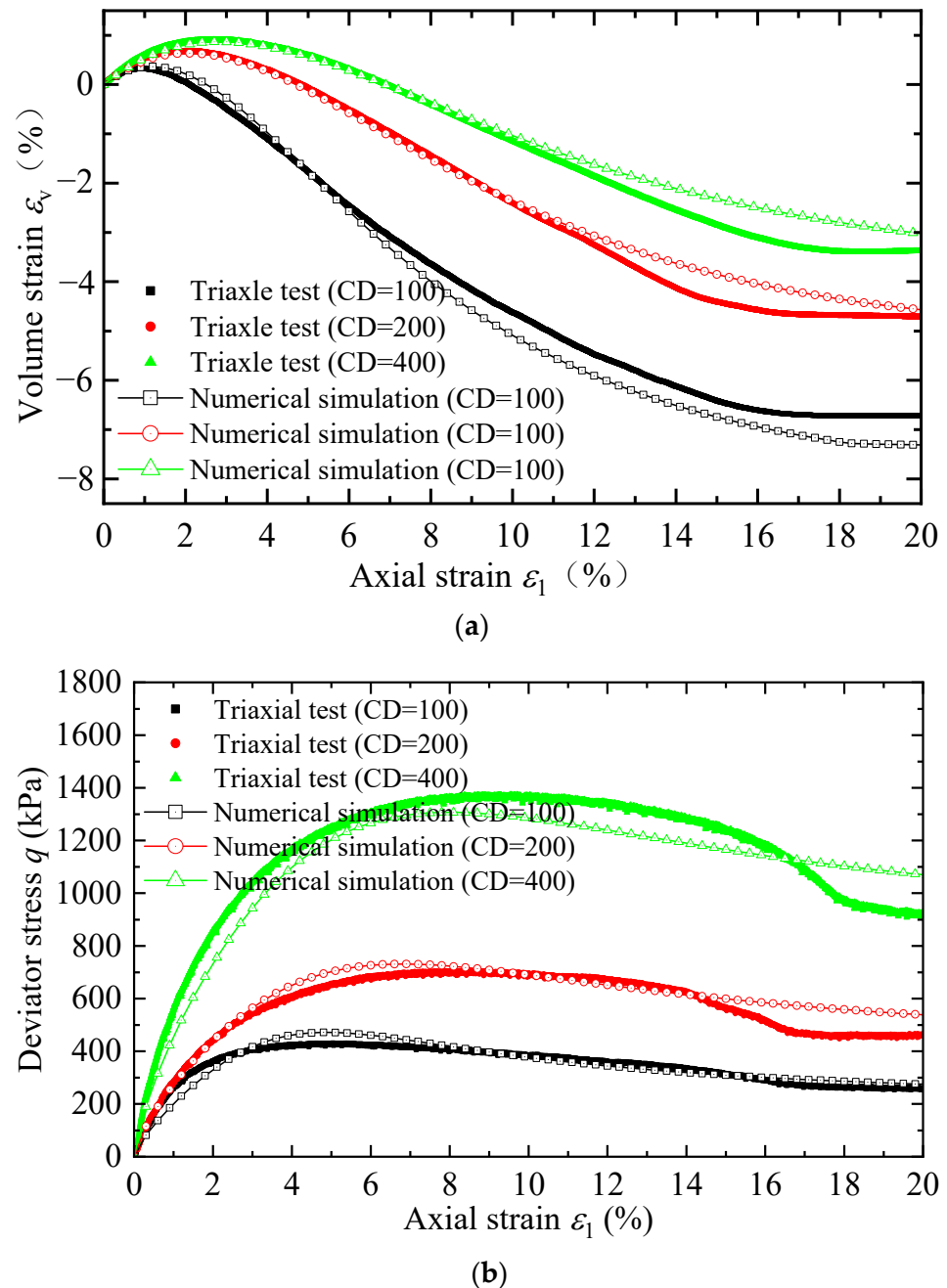


Figure 5. Comparison of triaxial consolidation drainage test and simulation results. (a) ε_v - ε_1 . (b) q - ε_1 .

It should be noted that, following Lashkari [21], other parameters for the model were also determined by matching the numerical simulation to the test results. All the calibrated parameters are summarized in Table 2.

Table 2. Parameter values of the calibrated SANISAND constitutive model.

Elastic Parameters	Critical State Parameters	Yield Surface Parameters	Plastic Modulus Parameters	Dilatancy Parameters	Fabric Dilatancy Tensor Parameters
$G_0 = 120$ $\nu = 0.2$	$M_c = 1.33$ $\lambda_c = 0.036$ $e_0 = 1.024$ $\xi = 0.7$	$m = 0.01$	$H_0 = 7.04$ $c_H = 0.989$ $n^b = 3.35$	$A_0 = 1.0$ $n^D = 1.2$	$z_{\max} = 4.0$ $c_z = 600$

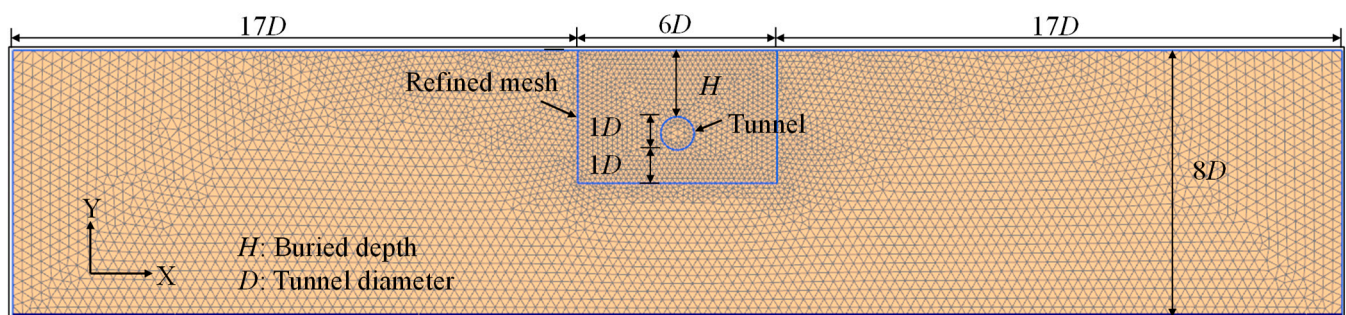
3. Establishment of Numerical Models

In this study, the ground deformation induced by the construction of super-large shield tunnels with a diameter (D) of 15 m is mainly studied. As the buried depth of most tunnels is within 50 m, three different ratios of the buried depth to the diameter (H/D), i.e., 1, 2, and 3, are investigated. However, to reveal the impact of soil compactness, seven types of sandy ground with different relative densities are considered. Therefore, 13 numerical cases are considered in total, as shown in Table 3.

Table 3. Numerical cases.

	$H/D = 1$	$H/D = 2$	$H/D = 3$
$D = 15$ m	$D_r = 30\%, 60\%, 90\%$	$D_r = 30\%, 40\%, 50\%, 60\%, 70\%, 80\%, 90\%$	$D_r = 30\%, 60\%, 90\%$

The software PLAXIS was utilized for numerical modeling. The size of the numerical model was set as $X_{\max} = 20 D$, $X_{\min} = -20 D$, $Y_{\max} = 0$, $Y_{\min} = -8 D$. The left and right boundaries of the model were fixed horizontally, the bottom was completely fixed, and the top boundary was free. The model is presented in Figure 6, in which fine meshes are used for soils adjacent to the tunnel. The SANISAND model with the parameters presented in Table 2 is used to describe the soil behavior. As the basic physical parameters of sand with different relative densities are different, the values of the void ratio and unit weight shown in Table 4 are specified for different cases. The tunnel shrinkage rate of 1.0% was used in simulations for all cases to reflect the overall soil loss due to excavation.

**Figure 6.** Two-dimensional numerical model.**Table 4.** Basic physical parameters for sand with different relative densities.

Relative Density, D_r	30%	40%	50%	60%	70%	80%	90%
Void ratio, e	0.981	0.939	0.897	0.854	0.812	0.770	0.728
unit weight, γ (kN/m ³)	13.38	13.67	13.97	14.29	14.62	14.97	15.33

4. Analysis of Numerical Results

4.1. Influence of the Ratio of Buried Depth to Diameter

In this section, the ground responses, including the displacement, the loss ratio, and the volume change characteristics, for the cases of $H/D = 1, 2, 3$ in sand with $D_r = 60\%$ are presented and compared, in order to investigate the impact of H/D .

4.1.1. Ground Displacement

Figure 7 compares the surface settlement trough after tunnel excavation for different H/D values. It can be seen that the trough becomes wider but shallower than the H/D increases. When $H/D = 1, 2,$ and 3 , the widths of the surface settlement trough are about $8D, 12D,$ and $16D$, respectively, and the maximum settlements are about $0.35\%D, 0.25\%D,$ and $0.18\%D$, respectively. It can be seen that the maximum settlement is nonlinearly related to H/D .

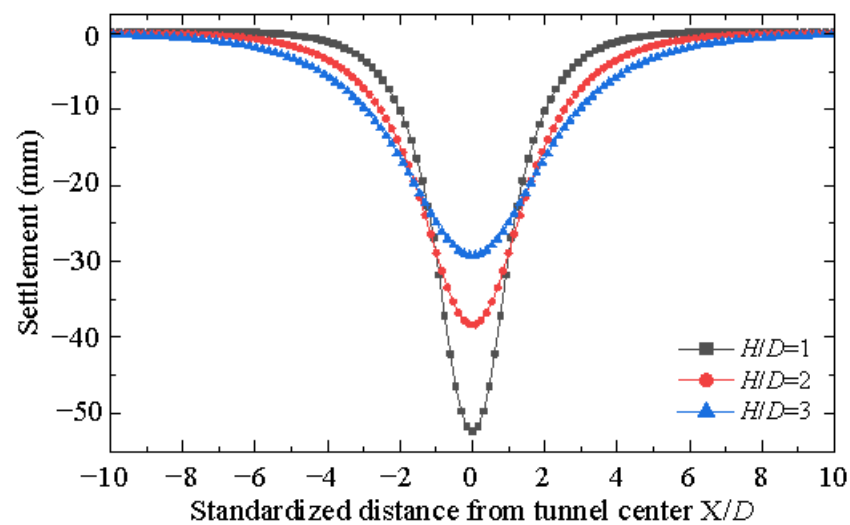


Figure 7. Settlement trough at the ground surface after tunnel excavation for different H/D values.

Figure 8 shows the distribution of the vertical displacement along the tunnel centerline for cases with different H/D values. In this figure, a negative value represents settlement, while a positive value represents the uplift. It can be seen that the shapes of the vertical displacement distribution curves are similar for the three cases. As the depth of soil decreases, the vertical displacement decreases first quickly and then slowly. The greater the H/D value, the smaller the change rate of the vertical displacement along the depth near the surface. The vertical displacement at the tunnel vault is 66 mm, 60 mm, and 54 mm for $H/D = 1, 2,$ and 3 , respectively. From the tunnel crown to the ground surface, the vertical displacement decreases by about 21% when $H/D = 1$. The reduction rate becomes 35% and 46% for $H/D = 2$ and $H/D = 3$, respectively. These results indicate that the larger the value of H/D , the smaller the vertical displacement at the vault induced by the tunnel excavation, and the greater the reduction in the vertical displacement when it is transferred to the surface.

Figure 9 presents the distribution of vertical stress along the depth after tunnel excavation for different H/D values. With the increase in H/D , the initial stress (the dashed line) around the tunnel increases linearly due to the self-weight of the soil. However, the tunnel excavation will cause greater stress release. The residual stress at the tunnel vault for different cases can be connected by a straight line passing through the origin after excavation, as shown in Figure 9. This indicates that the reduction in the vertical stress here is proportional to the buried depth of the tunnel. The maximum degree of reduction for all cases is about 45%.

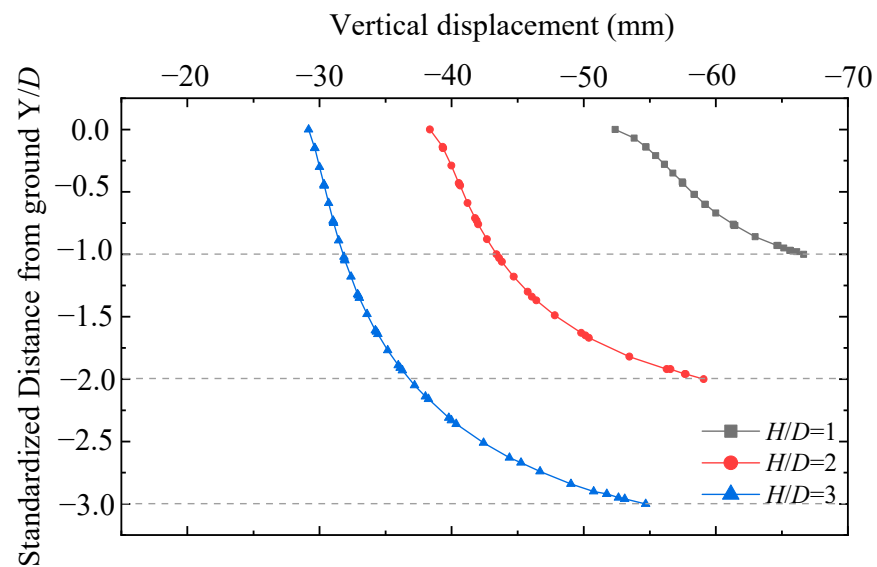


Figure 8. Distribution of the vertical displacement along the depth after tunnel excavation for different H/D values.

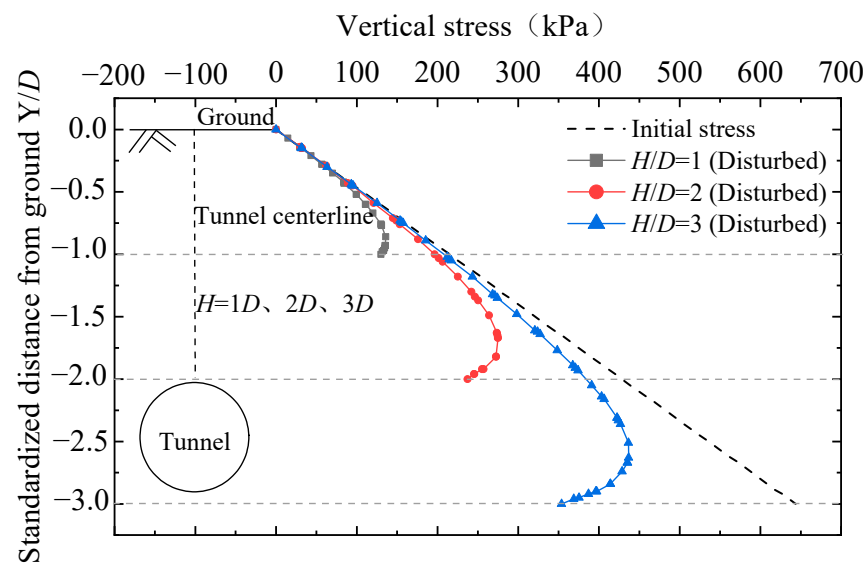


Figure 9. Vertical stress distribution along the depth after tunnel excavation for different H/D values.

4.1.2. Ground Loss Ratio

Based on the results of numerical analyses, the ground loss ratio at different depths can be calculated and is presented in Figure 10. It can be seen that, for the same depth, the ground loss ratio increases with increasing H/D . The ground loss ratio induced by the tunnel excavation is greater than the tunnel shrinkage rate (1.0%) at all depths. When $H/D=1$, the ground loss ratio at the vault is close to the tunnel shrinkage rate. With the increase in H/D , the ground loss ratio at the vault increases gradually.

When $H/D=1$, the ground loss ratio varies linearly along the depth. From the top of the tunnel to the surface, the formation loss ratio increases from 1.03% to 1.18% under $H/D=1$, from 1.11% to 1.28% when $H/D=2$, and from 1.16% to 1.32% when $H/D=3$. The differences between the rates at the ground surface and at the top of the tunnel are 0.15%, 0.17%, and 0.16% for the three cases, respectively. The phenomenon of an increase in the ground loss ratio from the tunnel to the ground surface is related to soil contraction behavior, which will be explained below.

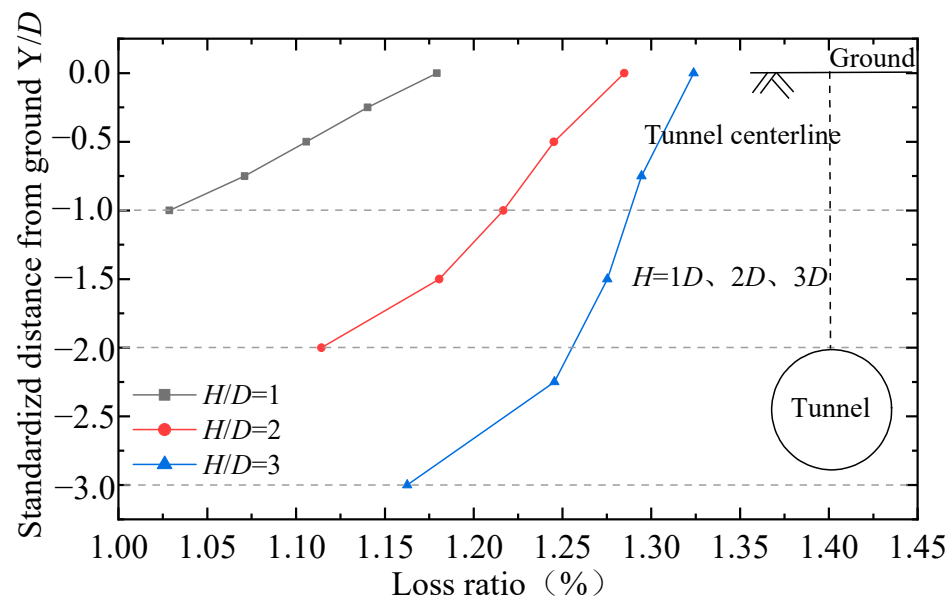


Figure 10. Distribution of stratum loss ratio along the depth after tunnel excavation with different coverage ratios.

4.1.3. Soil Volume Change

Figure 11 presents the contour of volumetric strain after tunnel excavation for different H/D values. It can be seen that the volumetric responses for soil mass vary significantly due to the excavation of tunnels at different depths. Overall, the soil contracts due to disturbance as a result of tunneling. The greater the buried depth, the smaller the overall volume change. When $H/D = 1$, the soil at the arch crown and the ground surface contracts greatly, but the soil around the haunch expands. As H/D becomes larger, the volume shrinkage of the soil at the vault and the surface is smaller, and the volume expansion of the soil at both sides of the surface and the haunch also becomes smaller.

Figure 12 shows the volume change due to tunnel excavation for different H/D values. When $H/D = 1$, the volumetric strains of soil at the surface, vault, and haunch are 0.12%, 0.28%, and -0.10% , respectively. When $H/D = 2$, the volumetric strains of the three soils are 0.09%, 0.22%, and -0.06% , respectively. When $H/D = 3$, the volumetric strains of the three soils are 0.06%, 0.20%, and -0.04% , respectively. The deeper the tunnel is buried, the smaller the volume shrinkage for the soil at the tunnel vault and at the surface, and the smaller the volume expansion for the soil at the tunnel haunch. Figure 11 indicates that, for all cases, the soils above the tunnel are subject to contraction; therefore, the ground loss ratio increases from the tunnel to the ground surface.

Figure 13 presents the evolution of the $e-p'$ state for soil at the tunnel haunch during excavation under different H/D . It can be seen from Figure 13 that when the tunnel is shallowly buried, the initial effective average stress at the haunch is small. After the disturbance by tunnel excavation, the effective average stress under the three cases decreases by about 18%, while the void ratios increase by 0.0019, 0.0012, and 0.0007 for $H/D = 1$, 2, and 3, respectively. It can be seen that the greater the buried depth of the tunnel, the smaller the change in the void ratio of the sand at the haunch. This is because the $e-p'$ state of the soil is located on the dense side of the critical state line initially. Shearing of soil will induce a dilatant response and the dilatancy will reduce as the confining pressure increases. Therefore, under a small H/D , the increase in the void ratio due to excavation-induced shearing will be more significant.

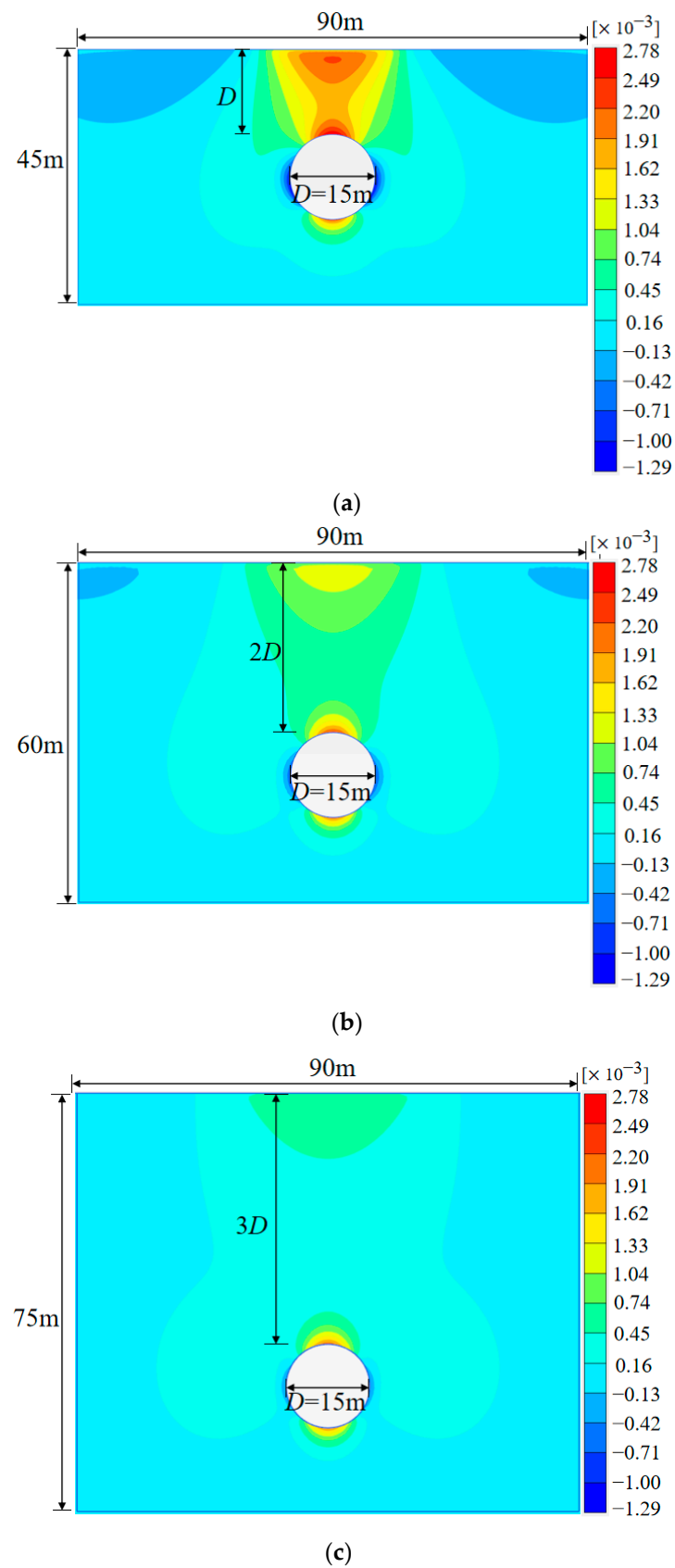


Figure 11. Volumetric strain contour after tunnel excavation for different H/D values. (a) $H/D = 1$. (b) $H/D = 2$. (c) $H/D = 3$.

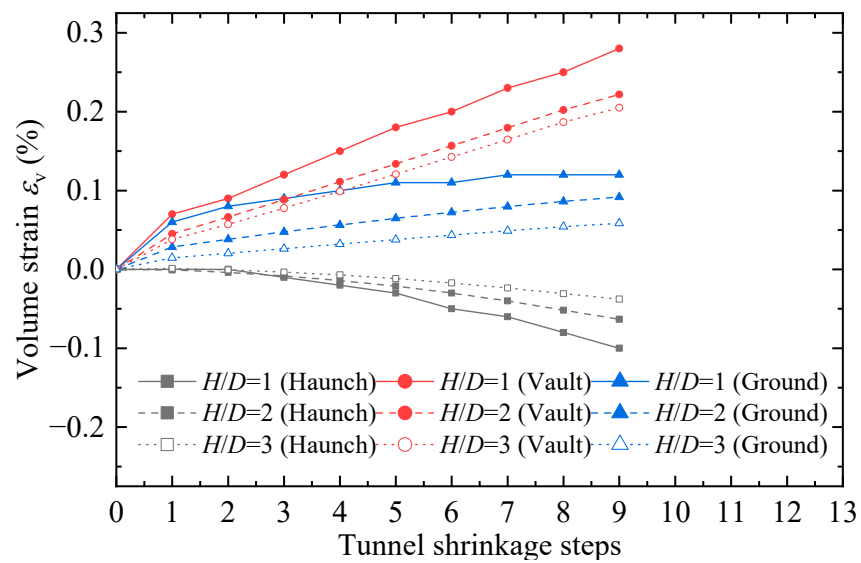


Figure 12. Volume change due to tunnel excavation for different H/D values.

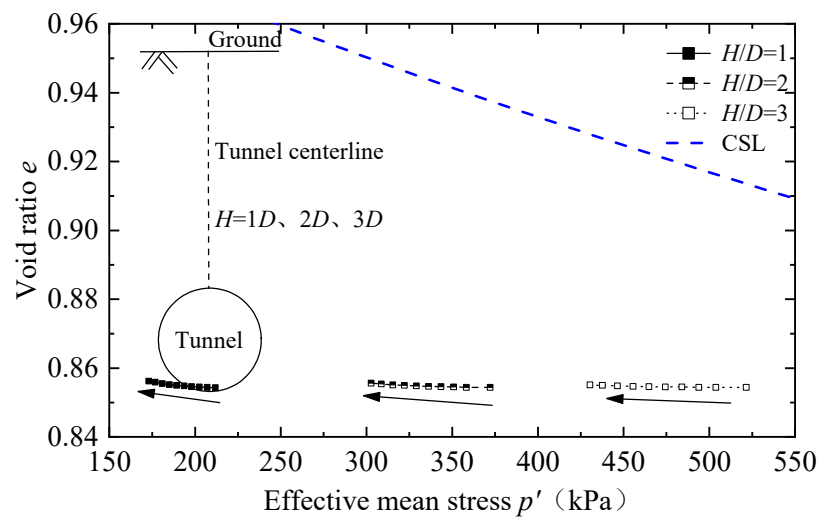


Figure 13. Evolution of $e-p'$ state for soil at the tunnel haunch during tunnel excavation for different H/D values.

4.2. Effect of Relative Density

To disclose the effect of the relative density of sand on the ground deformation induced by the tunneling, seven cases with $D_r = 30\% \sim 90\%$ were investigated for $H/D = 2$, while three cases with $D_r = 30\%$, 60% , and 90% were investigated for $H/D = 1$ and 3 . The results from the cases for $H/D = 2$ are presented in detail below.

4.2.1. Ground Displacement

Figure 14 presents the surface settlement trough after tunnel excavation for cases with relative density ranges from 30% to 90% . It can be seen that as the relative density is greater, the settlement becomes smaller, but the width of the surface settlement trough remains similar (about $12D$). The maximum settlement values are about 64.5 , 51.0 , 43.5 , 37.5 , 34.5 , 31.5 , and 30.0 mm, for $D_r = 30$, 40 , 50 , 60 , 70 , 80 , and 90% , respectively. As the sand becomes denser, the reduction rate in the settlement becomes smaller.

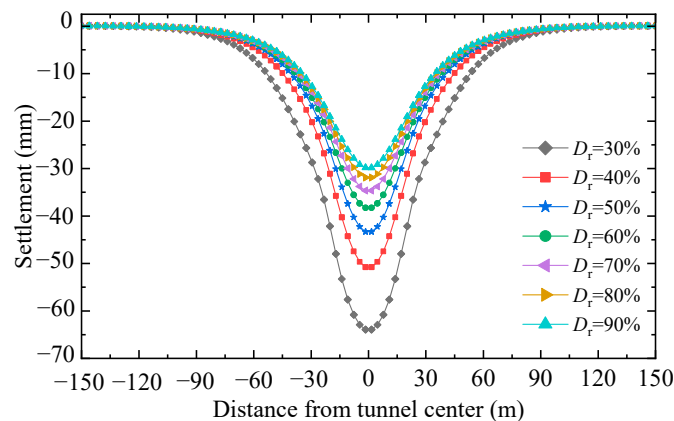


Figure 14. Surface settlement trough for sand layers with different relative densities.

In order to further analyze the ground deformation characteristics, the distribution of the vertical displacement along the depth for sandy ground with different relative densities is shown in Figure 15. It is worth mentioning that in all cases, the vertical displacement increases with the increase in depth. When the relative density increases from 30% to 40%, a significant reduction in the vertical displacement can be observed. As the relative density increases further, its impact on the vertical displacement response becomes less obvious. For example, the displacements at the top of the tunnel for the cases $D_r = 70, 80,$ and 90% are very close, being 58, 57, and 56 mm, respectively.

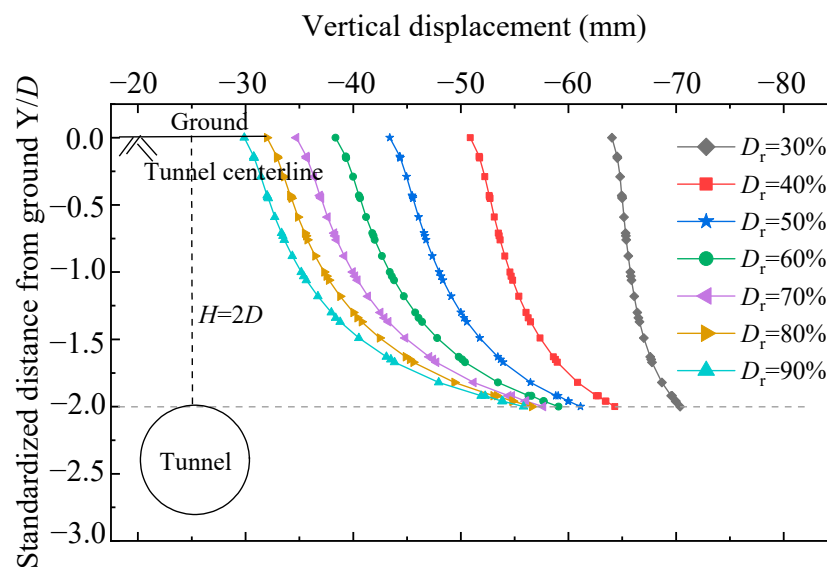


Figure 15. Distribution of vertical displacement along depth for sandy ground with different relative densities.

When $D_r = 30\%$, the vertical displacement of soil is the largest, but its degree of variation along the depth is the smallest. In this case, the vertical displacement at the top of the tunnel is 70 mm, and the vertical displacement on the surface is 64 mm (around 12% reduction). From the top of the tunnel to the surface, the vertical displacement is reduced by about 12%. With the increase in relative density, the difference between the vertical displacement at the top of the tunnel and that at the ground surface becomes larger. When $D_r = 90\%$, the vertical displacement decreases from 56 mm at the top of the tunnel to 30 mm at the ground surface, with a reduction rate of about 46%.

Figure 16 shows the distribution of the vertical stress increments along the depth due to tunneling in sandy ground with different relative densities. It can be observed that

significant stress reduction occurs around the tunnel due to excavation. The vertical stress reduces for soil within a $1 D$ range of the tunnel while increasing slightly for soil outside this range. The closer to the tunnel and the higher the relative density of the soil, the greater the stress release. This is because soil arching occurred above the the tunnel during excavation. For dense sand, it is easier to achieve stable arching under small disturbances.

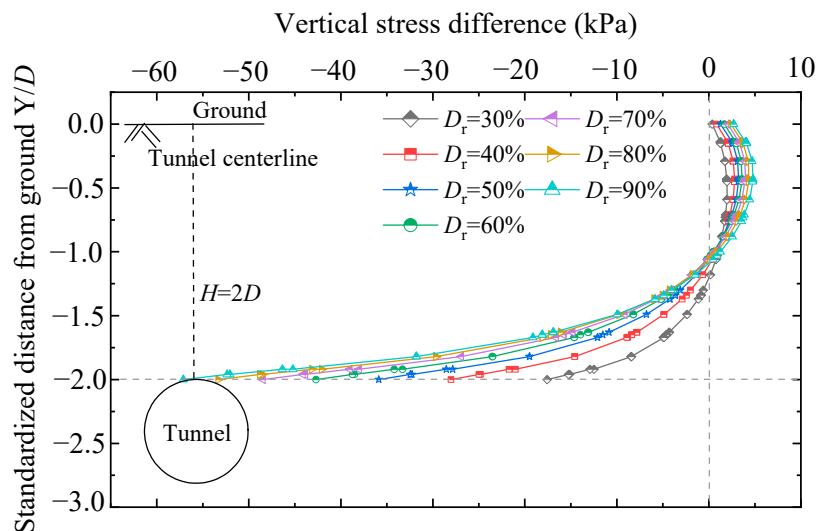


Figure 16. Distribution of the vertical stress increments along the depth due to tunneling in sandy ground with different relative densities.

4.2.2. Ground Loss Ratio

The distribution of the ground loss ratio along the depth for sandy ground with different relative densities is depicted in Figure 17. It can be seen that as the depth decreases, the ground loss ratio increases in all cases. The smaller the D_r , the greater the ground loss ratio, and the greater the degree of variation with depth. When $D_r = 30\%$, the ground loss ratio increases from 1.49% at the top of the tunnel to 2.35% at the ground surface, subject to an increase of 0.86%. When $D_r = 40\%$ – 90% , the ground loss ratio experiences increases of 0.43, 0.26, 0.17, 0.12, 0.08, and 0.05%, respectively, between the top of the tunnel and the ground surface. Compared to ground consisting of dense sand, ground consisting of loose sand is more susceptible to construction disturbance.

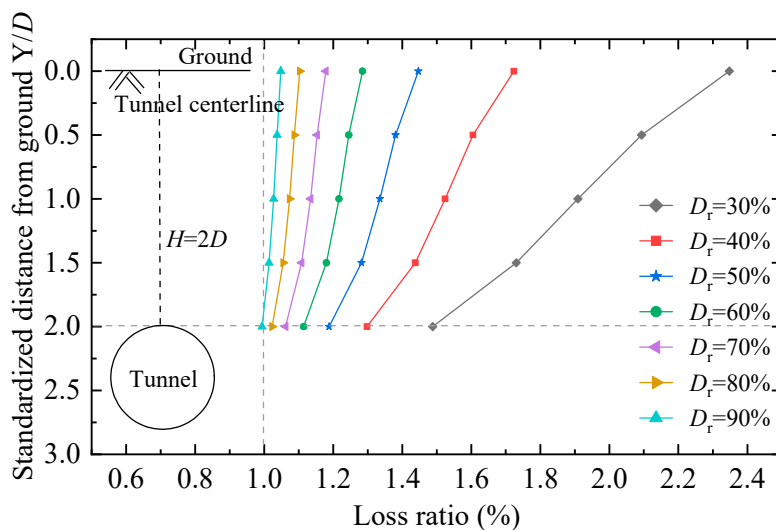


Figure 17. Distribution of ground loss ratio along depth for sandy ground with different relative densities.

4.2.3. Soil Volume Change

The distribution of the ground loss ratio along the depth, as presented in Figure 17, is highly correlated with the volumetric responses of sand during tunneling. Figure 18 shows the volumetric strain contour for ground with $D_r = 30, 60,$ and 90% . It can be seen that the soil above the tunnel is mainly subject to contraction and the volume strain decreases as the relative density increases. The soil on both sides of the tunnel is subject to contractions in the ground with $D_r = 30\%$ but dilation in the ground with $D_r = 60\%$ and 90% . As the relative density increases, the value and extent of the volume expansion increase.

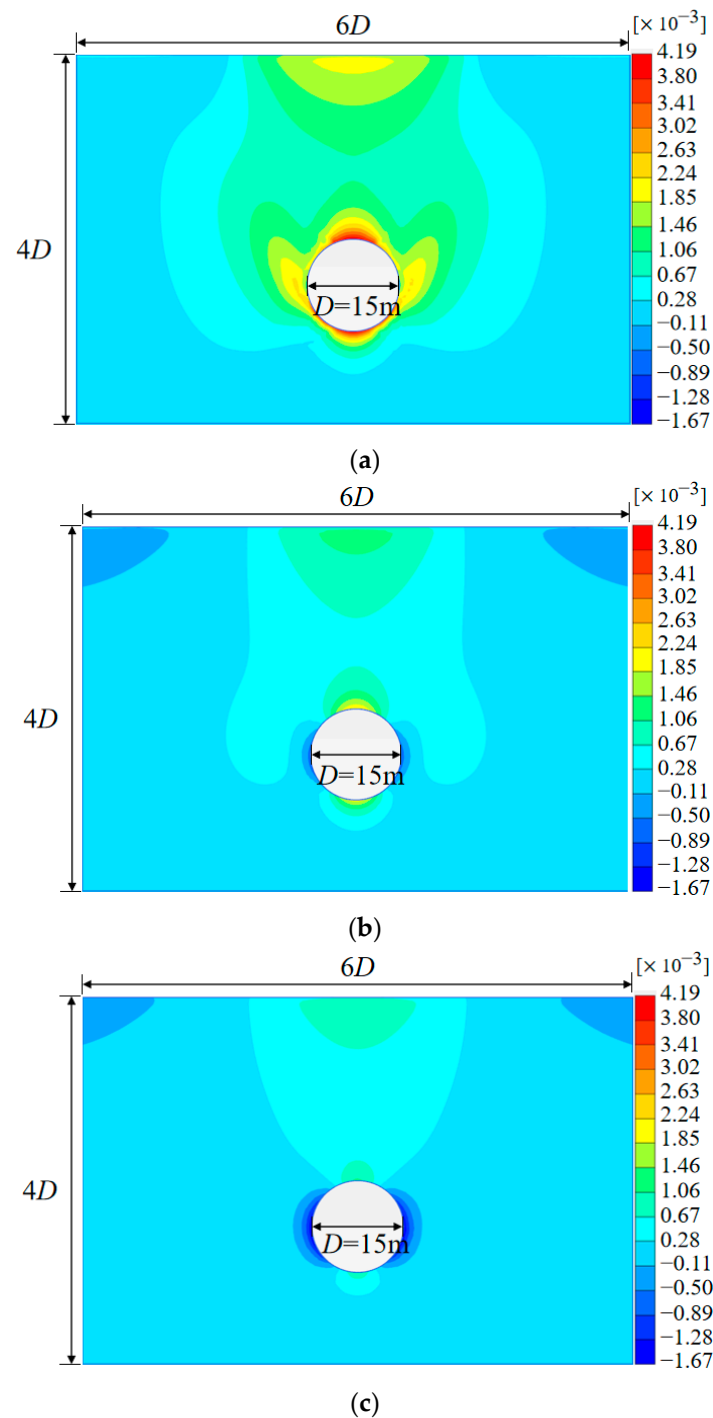


Figure 18. Volumetric strain cloud map for ground with different relative densities. (a) $D_r = 30\%$. (b) $D_r = 60\%$. (c) $D_r = 90\%$.

Figure 19 presents the volume strain distribution along the depth for ground with different relative densities. It can be seen that as the depth increases, the volumetric strain decreases first and then increases afterward. The volumetric strain at $1.2 D$ below the surface is the minimum. When $D_r = 30, 60,$ and 90% , the minimum volumetric strain $1.2 D$ below the surface is $0.1, 0.06,$ and 0.05% , respectively. The maximum volumetric strain at the top of the tunnel is $0.42, 0.23,$ and 0.12% . The volumetric strain at the ground surface is $0.13, 0.08,$ and 0.07% . From $1.2 D$ below the surface to the ground level, the volumetric strain of the three cases is reduced by about 0.02% . From $1.2 D$ below the ground surface to the top of the tunnel, the volumetric strain for the three cases increases by $0.32, 0.17,$ and 0.07% , respectively. For the cases of $D_r = 60\%$ and 90% , the soil on both sides of the tunnel experiences obvious volume expansion during the excavation of the tunnel. As shown in Figure 20, the maximum volumetric strain is -0.06% for $D_r = 60\%$, and -0.16% for $D_r = 90\%$. The results indicate that, due to less contractive response above the tunnel and dilative response on both sides of the tunnel, the ground loss rate will be much smaller in the ground comprising dense sand.

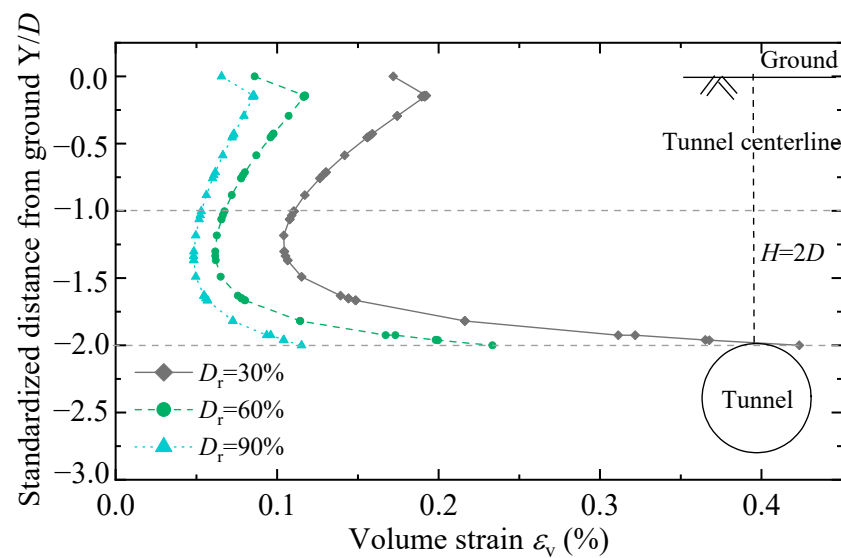


Figure 19. Volume strain distribution along depth for ground with different relative densities.

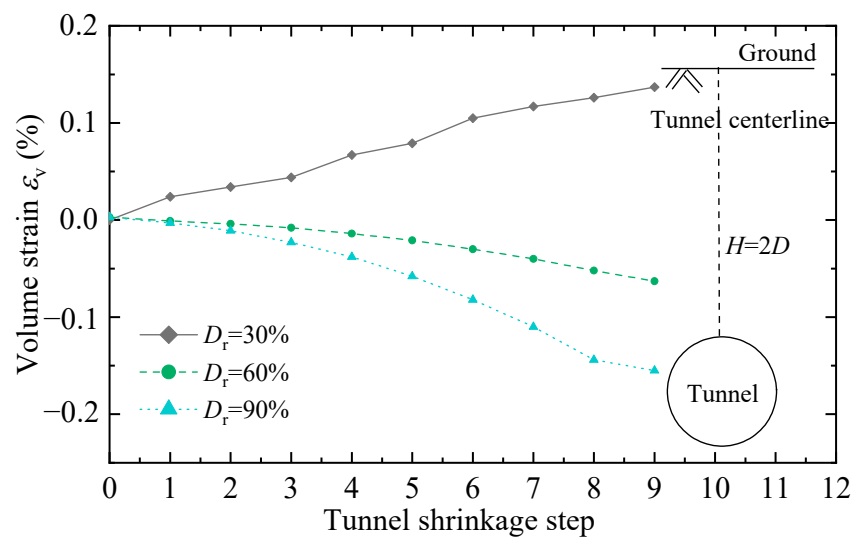


Figure 20. The volume change process of the soil around the haunch during tunnel excavation.

Figures 21 and 22 present q - p' and e - p' paths for the soil around the haunch during tunnel excavation. It can be seen from Figure 21 that after the disturbance of tunnel excavation, along with the decrease in the effective average stress of the soil at the haunch, the deviatoric stress decreases under $D_r = 30\%$ but increases under $D_r = 60\%$ and 90% . The sand at this location has approached the shear failure state due to the disturbance of tunnel excavation. From Figure 22, it can be seen that the effective average stress decreases, the void ratio of loose sand decreases, and the void ratio of dense sand and moderately dense sand increases due to sand shear expansion. The void ratio increases by 0.0012 and 0.0028 for medium-density and dense sand, respectively.

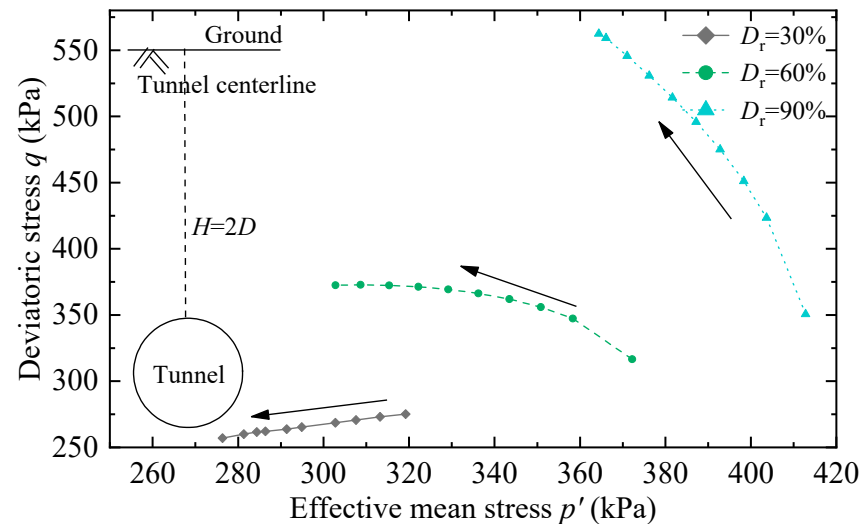


Figure 21. q - p' paths for soil around the haunch during tunnel excavation.

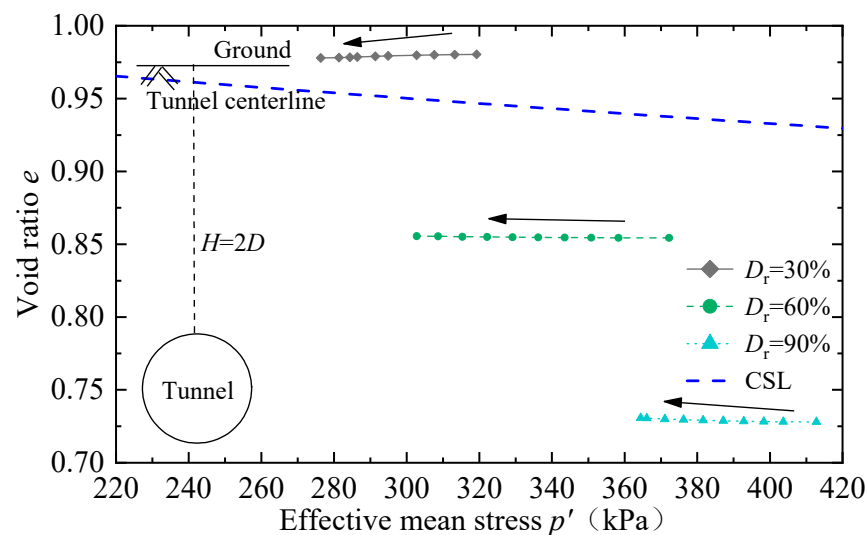


Figure 22. e - p' paths for soil around the haunch during tunnel excavation.

In summary, when the surrounding soil is disturbed by tunnel excavation, the greater the initial compactness of the sand, the stronger the ability to resist disturbance, and the smaller the value and extent of soil contraction. For the ground comprising dense sand, the shear-induced expansion around the tunnel haunch compensates part of the shear-induced contraction above the tunnel, so the overall ground loss ratio will be smaller than that in the ground comprising loose sand.

4.3. Impact of H/D and D_r on Parameters of Peck's Formula

In 1969, Peck [2] proposed a formula to predict surface subsidence,

$$S(x) = S_{\max} \exp\left(-\frac{x^2}{2i^2}\right) \quad (6)$$

$S(x)$ is the vertical distance from the initial surface position to the settlement trough for the point with a distance of x from the tunnel center; S_{\max} is the maximum vertical distance between the settlement trough and the initial surface, which generally occurs at the surface above the center of the tunnel axis; i is the width of the settlement trough, defined as the distance between the symmetrical center of the curve and the reverse bending point.

Equation (6) shows that the shape of Peck's curve is determined by the width of settlement trough i and the maximum surface settlement S_{\max} . In this section, the results from numerical analysis are utilized to study the influence of the relative density, and the ratio of the buried depth to tunnel diameter on both i and S_{\max} .

Table 5 shows the width of the settlement trough, i , for nine different cases. From the data, it can be seen that i increases significantly with the ratio of buried depth to diameter, H/D . When H/D increases from 1 to 3, the value of i increases by 66.7% to 111.6%. However, the relative density has a less significant influence on parameter i , especially for the cases of $H/D = 3$.

Table 5. The width of settlement trough, i , in different cases (unit: m).

D_r	$H/D = 1$	$H/D = 2$	$H/D = 3$
30%	19.37	25.88	32.29
60%	15.92	23.52	31.75
90%	16.03	24.71	33.92

Table 6 summarizes the maximum settlement at the ground surface in different cases. It can be seen from the table that S_{\max} is negatively correlated with both H/D and D_r . As H/D increases from 1 to 3, S_{\max} decreases by 21.3, 44.6, and 48.7% for ground with $D_r = 30$, 60, and 90%, respectively.

Table 6. The maximum settlement, S_{\max} , in different cases (unit: mm).

D_r	$H/D = 1$	$H/D = 2$	$H/D = 3$
30%	68.8	61.2	54.2
60%	50.1	36.4	27.7
90%	41.3	28.4	21.2

Finally, by use of the data presented in Tables 5 and 6, the following formula for predicting i and S_{\max} of the settlement curve as induced by the excavation of a tunnel with a diameter of 15 m can be obtained as follows:

$$i = 7.77H/D + 9.27 \text{ (m)} \quad (7)$$

$$S_{\max} = -9.9H/D + 47.2D_r^{-0.45} \text{ (mm)} \quad (8)$$

5. Conclusions

By incorporating the SANISAND constitutive model, which can reproduce the behavior of sand under various combinations of density and confining pressure, numerical analyses were conducted to investigate the deformation characteristics of sandy ground induced by the tunneling of a super-large-diameter shield. The impact of the relative density of sand (D_r) and the ratio of the buried depth to tunnel diameter (H/D) were revealed. From the study, the following conclusions can be drawn:

- (1) The width of the settlement trough at the ground surface is highly correlated with H/D . The half-width of the trough is about $4D$, $6D$, and $8D$ for the cases of $H/D = 1$, 2 , and 3 , respectively. However, for the same H/D , D_r has no obvious impact on the width.
- (2) The maximum settlement at the ground surface as induced by tunneling depends on both H/D and D_r . For the same D_r , the maximum settlement decreases with the increase in H/D . For the same H/D , the maximum settlement decreases with the increase in D_r .
- (3) Along the centerline of tunneling, the vertical displacement (settlement) above the tunnel decreases with increasing distance from the tunnel. When H/D and D_r are larger, the “loss” in the vertical displacement becomes greater when it approaches the ground. When $D_r = 60\%$, the loss is about 21 , 35 , and 46% for the cases of $H/D = 1$, 2 , and 3 , respectively.
- (4) The ground loss ratio increases with increasing distance from the tunnel, and its variation depends on the relative density of the ground soil. From the top of the tunnel to the ground surface, the ground loss ratio increases by 0.86 , 0.43 , 0.26 , 0.17 , 0.12 , 0.08 , and 0.05% for ground consisting of sand with relative densities of 30 , 40 , 50 , 60 , 70 , 80 , and 90% .
- (5) In all cases, the soil above the tunnel is mainly subject to contraction. For the ground comprising dense sand, the shear-induced expansion around the tunnel haunch compensates for part of the shear-induced contraction above the tunnel, so the overall ground loss ratio is smaller than that in the ground comprising loose sand.

Author Contributions: Conceptualization, J.L. and X.L.; methodology, D.S.; software, Y.W.; validation, J.L.; formal analysis, X.L.; investigation, Y.W.; resources, D.S.; data curation, D.S.; writing—original draft preparation, Y.W.; writing—review and editing, D.S.; visualization, X.L.; supervision, J.L.; project administration, J.L.; funding acquisition, D.S. All authors have read and agreed to the published version of the manuscript.

Funding: This research work was funded by the National Natural Science Foundation of China (Grant Nos. 52090081 & 51938008), the Natural Science Foundation of Shenzhen (Grant No. JCYJ2021032 4094607020), and the Key Research and Development Project of Guangdong Province (Grant No. 2019B111105001).

Data Availability Statement: Not applicable.

Conflicts of Interest: The authors declare no conflict of interest.

References

1. Fang, Y.; Chen, Z.; Tao, L.; Cui, J.; Yan, Q. Model Tests on Longitudinal Surface Settlement Caused By Shield Tunnelling in Sandy Soil. *Sustain. Cities Soc.* **2019**, *47*, 101504. [[CrossRef](#)]
2. Peck, R.B. Deep Excavation and Tunnelling in Soft Ground. In Proceedings of the 7th International Conference on Soil Mechanics and Foundation Engineering, State of the Arts Volume, Mexico City, Mexico, 1969.
3. Fattah, M.Y.; Shlash, K.T.; Salim, N.M. Prediction of settlement trough induced by tunneling in cohesive ground. *Acta Geotech.* **2013**, *8*, 167–179. [[CrossRef](#)]
4. Song, Z.; Tian, X.; Zhang, Y. A new modified Peck formula for predicting the surface settlement based on stochastic medium theory. *Adv. Civ. Eng.* **2019**, *2019*, 7328190. [[CrossRef](#)]
5. Zhou, J.; Chen, D.; Wang, D.; Zhang, L.L.; Zhang, L.M. Failure probability of transverse surface settlement induced by EPB Shield tunneling in clayey soils. *ASCE-ASME J. Risk Uncertain. Eng. Syst. Part A Civ. Eng.* **2018**, *4*, 04018030. [[CrossRef](#)]
6. Wei, Z.; Zhu, Y. A theoretical calculation method of ground settlement based on a groundwater seepage and drainage model in tunnel engineering. *Sustainability* **2021**, *13*, 2733. [[CrossRef](#)]
7. Tang, X.; Liang, J.; Liu, W.; Ye, Y.; Gan, P.; Zhao, W.; Yu, Y. Modification of Peck Formula to Predict Ground Surface Settlement of Twin Tunnels in Low Permeability Soil. *Adv. Civ. Eng.* **2021**, *2021*, 6698673. [[CrossRef](#)]
8. Li, Y.; Lin, J.; Yan, S.; Du, J. Modification of the Peck Formula for a Double-Track Shield Tunnel under Expressway Subgrade. *Symmetry* **2022**, *14*, 1904. [[CrossRef](#)]
9. Do, N.A.; Dias, D.; Oreste, P. 3D numerical investigation of mechanized twin tunnels in soft ground—Influence of lagging distance between two tunnel faces. *Eng. Struct.* **2016**, *109*, 117–125. [[CrossRef](#)]

10. Zhang, T.; Nie, L.; Zhang, M.; Dai, S.; Xu, Y.; Du, C.; Rui, X.; He, Y. The unsymmetrical coefficient of unsymmetrical-loaded tunnel based on field monitoring and numerical simulation. *Symmetry* **2020**, *12*, 1793. [[CrossRef](#)]
11. Ağbay, E.; Topal, T. Evaluation of twin tunnel-induced surface ground deformation by empirical and numerical analyses (NATM part of Eurasia tunnel, Turkey). *Comput. Geotech.* **2020**, *119*, 103367. [[CrossRef](#)]
12. Khaksari, R.; Harun, Z.; Fielding, L.; Aldridge, J. Numerical Simulation of the Evacuation Process in a Tunnel during Contraflow Traffic Operations. *Symmetry* **2021**, *13*, 2392. [[CrossRef](#)]
13. Zhang, Z.X.; Zhang, H.; Yan, J.Y. A case study on the behavior of shield tunneling in sandy cobble ground. *Environ. Earth Sci.* **2013**, *69*, 1891–1900. [[CrossRef](#)]
14. Zhang, P.; Pan, Y.; Yu, Z.; Guan, X.; Wang, G.; An, J.; Lei, H. Ground subsidence characteristics caused by construction of shallow-buried tunnel in a sandy soil composite formation. *Arab. J. Geosci.* **2020**, *13*, 901. [[CrossRef](#)]
15. Hu, X.; He, C.; Peng, Z.; Yang, W. Analysis of ground settlement induced by Earth pressure balance shield tunneling in sandy soils with different water contents. *Sustain. Cities Soc.* **2019**, *45*, 296–306. [[CrossRef](#)]
16. Moussaei, N.; Khosravi, M.H.; Hossaini, M.F. Physical modeling of tunnel induced displacement in sandy grounds. *Tunn. Undergr. Space Technol.* **2019**, *90*, 19–27. [[CrossRef](#)]
17. Sun, J.; Liu, J. Visualization of tunnelling-induced ground movement in transparent sand. *Tunn. Undergr. Space Technol.* **2014**, *40*, 236–240. [[CrossRef](#)]
18. Lu, H.; Shi, J.; Wang, Y.; Wang, R. Centrifuge modeling of tunneling-induced ground surface settlement in sand. *Undergr. Space* **2019**, *4*, 302–309. [[CrossRef](#)]
19. Dafalias, Y.; Manzari, M. Simple Plasticity Sand Model Accounting for Fabric Change Effects. *J. Eng. Mech.* **2004**, *130*, 622–634. [[CrossRef](#)]
20. Taiebat, M.; Dafalias, Y. Sanisand: Simple Anisotropic Sand Plasticity Mode. *Int. J. Numer. Anal. Methods Geomech.* **2008**, *32*, 915–948. [[CrossRef](#)]
21. Lashkari, A. A Sanisand Model with Anisotropic Elasticity. *Soil Dyn. Earthq. Eng.* **2010**, *30*, 1462–1477. [[CrossRef](#)]

Disclaimer/Publisher’s Note: The statements, opinions and data contained in all publications are solely those of the individual author(s) and contributor(s) and not of MDPI and/or the editor(s). MDPI and/or the editor(s) disclaim responsibility for any injury to people or property resulting from any ideas, methods, instructions or products referred to in the content.